EUROPEAN ORGANIZATION FOR NUCLEAR RESEARCH

CERN–SL/97–59 BI

Synchrotron radiation interferences between short dipoles at LEP

C. Bovet, A. Burns, F. Méot[*], M. Placidi, E. Rossa, J. de Vries

CERN, Geneva, Switzerland.

Abstract

A dedicated Synchrotron Radiation source operates in the near-UV to visible range for 3D diagnostics on the LEP e^+ and e^- beams with a streak camera as part of the beam instrumentation equipping the storage ring. A first four-dipole configuration (**mini-wiggler**) exploited until 1993 presented mutual interferences between sources in the spectral range in use and had unwanted multiple source effects on the image formation. Experimental and theoretical investigations on time coherence effects from neighbouring magnets led to a new configuration which provides significantly higher light intensity and improved beam imaging.

Geneva, Switzerland

December 2, 1997

[*]CEA/DSM/DAPNIA, SEA, CEA, Saclay, 91191 Gif-sur-Yvette, France.

1 Introduction

Two insertion devices (**mini-wigglers**) [1] provide dedicated synchrotron radiation (SR) for transverse and longitudinal beam profile measurements in LEP with a streak camera sensitive in the near-UV to visible range [2]. Synchrotron light beams are produced by electrons and positrons in two identical mini-wiggler setups located at ~ 67 m on either side of IP1.

A first configuration exploited until 1993 (Fig. 1) involved a $\sim$ 3 m long localised closed orbit bump fully compatible with the several modes of operation of the machine. This configuration however presented unwanted multiple source effects and strong destructive interferences reducing the light intensity in the low-frequency range of the spectrum.

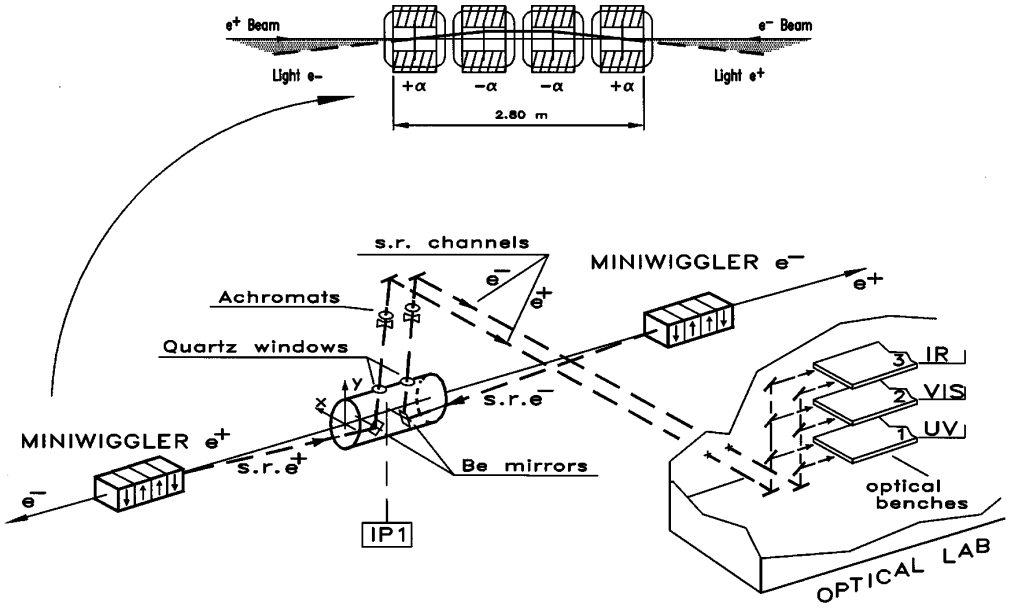

Figure 1: The very first mini-wiggler set-up in the LSS1 LEP straight section. e^+e^- synchrotron light beams are deflected by two beryllium mirrors close to IP1 and focused by two achromat lenses onto the image planes in the optical laboratory.

Experiments with different mini-wiggler configurations were performed in 1993 and 1994 in order to assess the interference phenomenon and investigate the possibility of better separating the selected light source from those originating in the neighbouring magnets.

Experimental results [3] are compared to theoretical predictions [4] in Fig. 2 which shows the evolution of the light intensity at the streak camera as a function of the dipole excitation for each of the three configurations investigated. The three configurations were, either a single dipole, entailing a closed orbit bunp extending from the e^- to the e^+ miniwiggler; either a closed orbit shift, closed

elsewhere with orbit correctors, (‘ $-\,-\,+\,+$’ case); either a local 3 meters long closed orbit bunp (Fig. 1), (‘ $+\,-\,-\,+$’ case).

The main comments relevant to both the measurements and the numerical simulations are as follows. In the single dipole case there is a fast increase of the intensity as a function of the dipole current. On the contrary in the ‘ $+\,-\,-\,+$’ 4-dipole case the intensity is almost constant from 10 to 40 amperes. The ‘$--++$’ case shows an intermediate behaviour. Measurements in the single dipole case with up to 40 A dipole current, involving light attenuation with grey filters, not reported here, showed a light intensity improvement of about a factor of 100 with respect to the ‘ $+\,-\,-\,+$’ case.

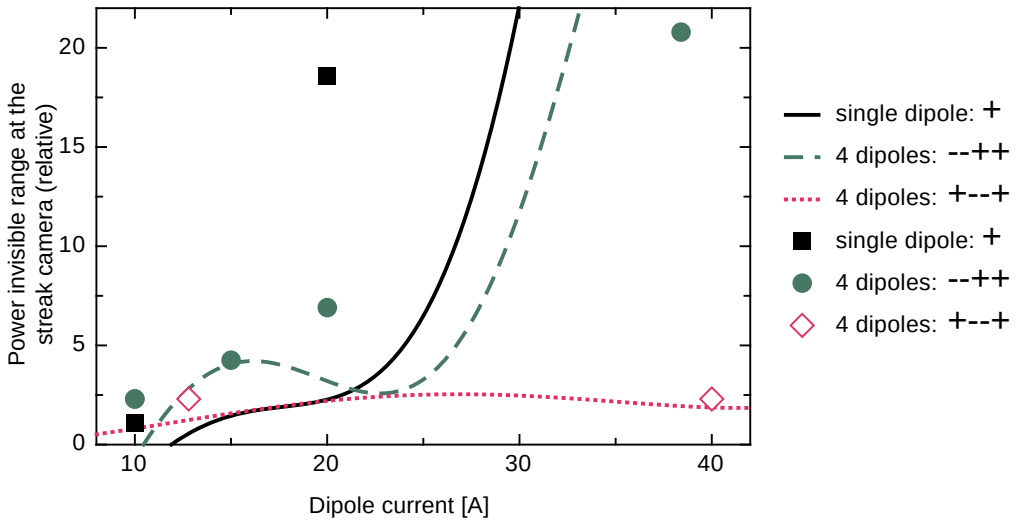

Figure 2: Summary of the experimental data [3] and comparison with numerical simulations (continuous curves, Appendix 5 of Ref. [4]) performed in 1993 and 1994. The radiated power at the streak camera is shown as a function of the dipole excitation for two different 4-dipole configurations and for the single-dipole case.

2 The new mini-wiggler configuration

The new set-up has been designed to cope with the LEP bunch-train optics involving vertical closed orbit bumps at the eight symmetry points of the LEP structure to avoid unwanted encounters between counterrotating bunches [5]. Theoretical investigations on possible geometric configurations have shown that magnets with opposite field too close to the selected source can generate prohibitive interference [4]. In particular the nearby doublet QL4, which is inside the vertical bump required for beam separation in the bunch train scheme, provides a considerable amount of parasitic radiation as shown in the interference plots of Fig. 3.

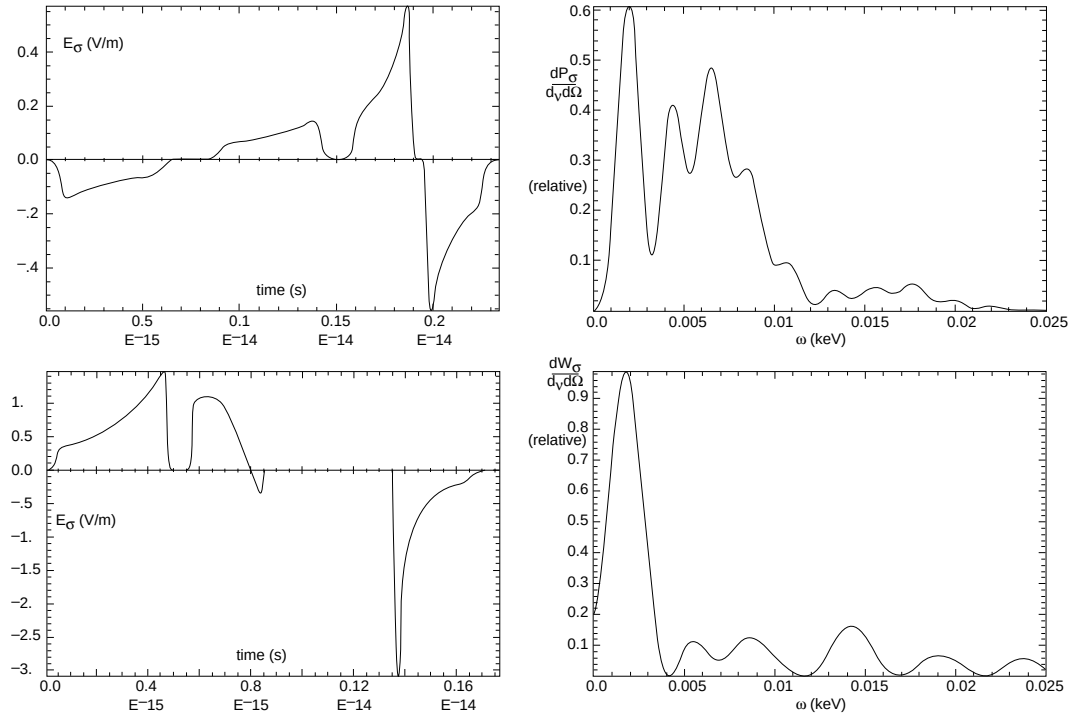

Figure 3: Numerical simulation of the mutual interference between the mini-wiggler dipoles and the neighbouring magnets. The figure shows the E_σ electric field component of the SR electromagnetic wave (polarization parallel to the orbit plane) emitted by a 45 GeV electron, as observed at large distance in the direction of the imaging optics (left-hand graphs) and the corresponding component of the spectral brightness (right-hand graphs) as emitted in
a) the first mini-wiggler set-up with $\alpha = 0.2$ mrad deflection in the dipoles (Fig. 1) (top),
b) a doublet SR source made of a single small dipole and the QL4 doublet (bottom).
The oscillatory nature of the spectra reveals the interferential behaviour of the SR emission in the magnet sequence.

2.1 Implementation and closed-orbit bump

The above investigations led to the new configuration now operational in LEP shown in Fig. 4. involving four dipoles identical to those used in the previous set-up, whose characteristics are recalled in Table 1.

The e^+ and e^- synchrotron light beams from W3 and W4 are deflected by two beryllium mirrors close to IP1 and focused by two achromat lenses onto the streak camera located in the optical laboratory as in the original version. To provide equal path lengths for the two light beams to the image plane the extraction mirrors are asymmetrically positioned w.r.t. IP1 to have the e^+ light extracted earlier as required by the position of the optical benches in the laboratory (Fig. 1). The local closed orbit bump associated with the new arrangement stretches over 15.6 m (Fig. 5) and includes the horizontally defocusing doublet QL4.

Table 1: Characteristics of the new mini-wiggler insertions

DIPOLES		
Physical length	m	0.680
Magnetic length	m	0.526
Maximum dipole (PC) current	A	60 (55)
Maximum field (field strength)	T (Tm)	0.266 (0.14)
Power	kW/dipole	4.5
PERFORMANCE		
Nominal excitation	A/GeV	0.61
Nominal dipole deflection ($E \leq 90$ GeV)	mrad	$\alpha = 0.43$
Radius of curvature	m	$\rho = 1223.3$
Critical energy at 45 (90) GeV	keV	$\omega_c = 165.3$ (1322)
Critical wavelength at 45 (90) GeV	10^{-3} nm	$\lambda_c = 7.5$ (0.94)
Maximum deflection at 45 GeV	mrad	0.86
Maximum deflection at 100 GeV	mrad	0.39
LAYOUT and OPTICAL SET-UP (distances between centres)		
W1—QL4B—QL4A—W2—W3—W4	m	2.5 / 2.1 / 2.835 / 1.4 / 6.751
W3–mirror / W4–mirror (e^+-line)	m	66.598 / 59.847
W3–mirror / W4–mirror (e^--line)	m	66.771 / 60.020
Full bump length (W1—W4)	m	15.586
Nominal bump amplitude	mm	δx = 2.9
Achromat focal length	m	15.708 at $\lambda = 546$ nm
Achromat–image plane (optical laboratory)	m	20.320±0.375
W3–achromat / W4–achromat	m	67.771±0.375 / 61.020±0.375
W3–image plane / W4–image plane	m	88.091 / 81.340
Physical (projected) mirror size	mm^2	68.0×120.0 (68.0×85.0)
Mirror–beam clearance	mm (σ_x)	14.0 ($13 \div 16$)
Angle optics axis to beam axis	mrad	$\varphi = 0.80$

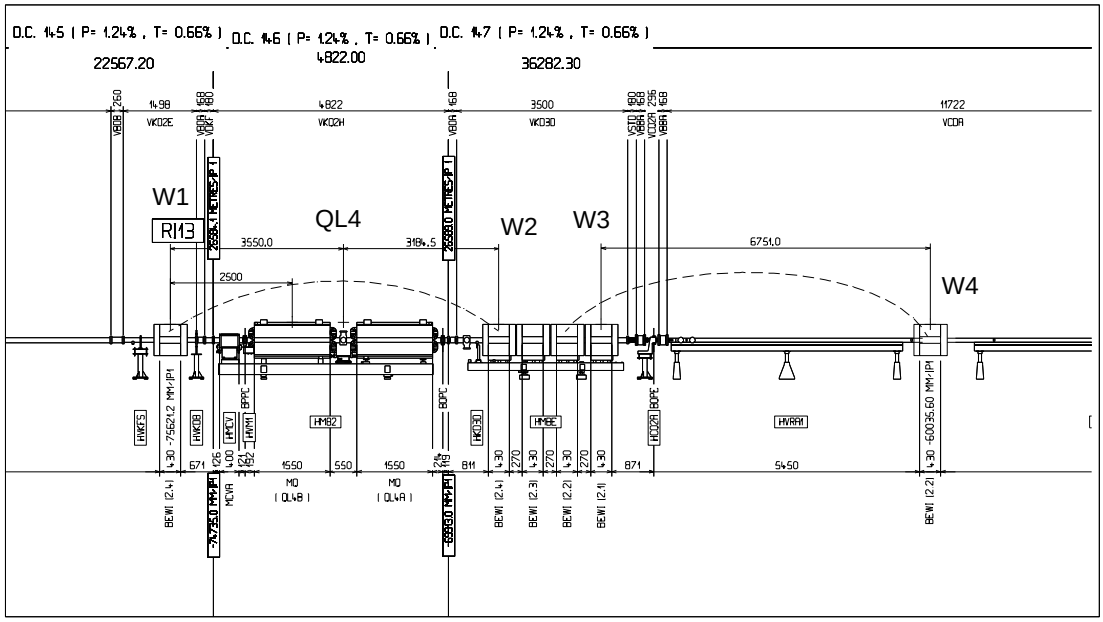

Figure 4: The new mini-wiggler layout at the left side of IP1 for diagnostics on the e^+ beam. A similar set-up is installed symmetrically to IP1 for the e^- beam. SR from both dipoles W3 and W4 fall within the acceptance of the imaging optics (shown schematically in Fig. 6). However, the useful SR source onto which the imaging optics is to focus is W4; the effect of W3 is then reduced to a $\sim 10\%$ parasitic blurring (Appendix 1).

The nominal deflections ($\alpha = 0.43$ mrad) of the dipoles W2, W3 and W4 produce a 2.9 mm bump amplitude between W2 and W3. The bump is closed by matching the W1 deflection $\alpha_{\rm w1}$ to take into account the deflection $\alpha_{\rm QL}$ produced in the double quadrupole QL4 so that

$$\alpha = \alpha_{\rm w1} + \alpha_{\rm QL} = \alpha_{\rm w1}\big[1 - (KL)(2l_1 + l_2) + (KL)^2 l_1 l_2\big] \qquad (1)$$

where $(KL) = -0.02876$ m^{-1} is the strength of QL4A and QL4B for the LEP optics under consideration (90°/60°, and 108°/90°) and l_1, l_2 the distances W1–QL4B and QL4B–QL4A (Table 1).
With the layout of Fig. 4 we have from (1) $\alpha_{\rm w1} = 0.827\ \alpha$. As the deflection $\alpha_{\rm QL}$ in the QL4 doublet is proportional to $\alpha_{\rm w1}$, obtained with a shunt resistance across W1, the bump is closed whatever the beam energy and for any mini-wiggler setting. Values of α up to 1.4 mrad have been used during the parasitic tests at injection energy in 1995.

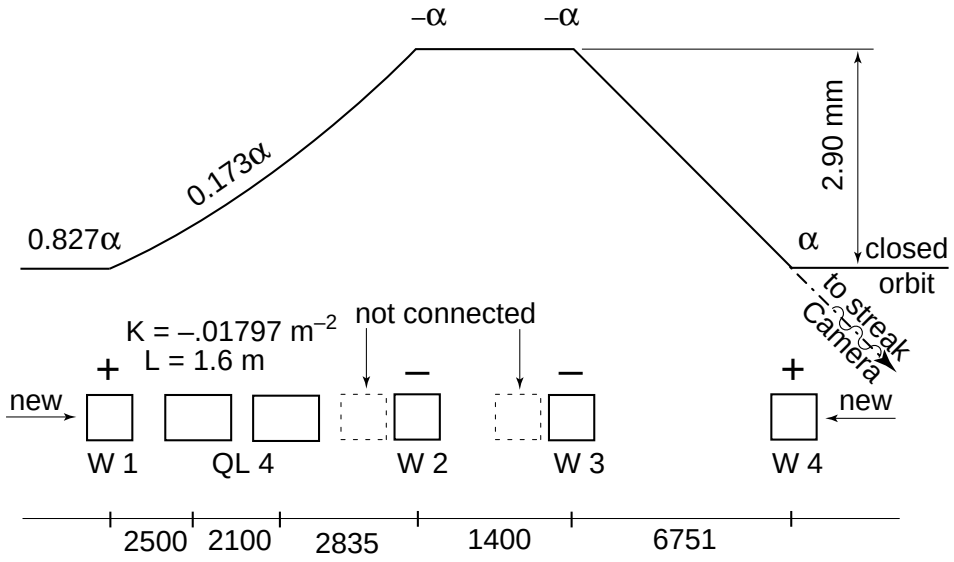

Figure 5: The horizontal closed-orbit bump produced by the new mini-wiggler set-up stretches over 15.6 m between the two extreme dipoles W1 and W4. The doublet QL4 contributes to the bump together with the dipole W1 for any beam energy and bump amplitude, independently of any non-zero vertical closed orbit which is the case in the bunch train mode of operation. The trajectory in the last two dipoles W3, W4 is aligned with the axis of the imaging optics to allow the superposition of the two light spots at the image plane.
The nominal deflection $\alpha = 0.43$ mrad requires $I = 55$ A at 90 GeV.

2.2 Mini-wiggler geometry

The most powerful SR source from the imaging view point is the dipole W4. Its light is received through the centre of the focusing achromat at an angle $\varphi = 0.8$ mrad to the beam axis (Fig. 6).

At the nominal settings the light from W3 is also intercepted by the imaging optics, while the parasitic SR sources from W1, QL4, and W2 fall outside the acceptance of the optic channels for deflections $\alpha > 0.4$ mrad.

The drawback of having a double source W3-W4 is attenuated in two steps. The camera is first focused onto the source W4, the optical field depth being short enough to reduce the contribution from the source W3 to a quasi uniform 10% background (Appendix 1). The deflections in W3 and W4 are then tuned to either align the two sources on the imaging optics axis (Fig. 6) i.e. superimposing the two light spots on the image plane, or on the contrary, fully separate them by means of large deflection α.

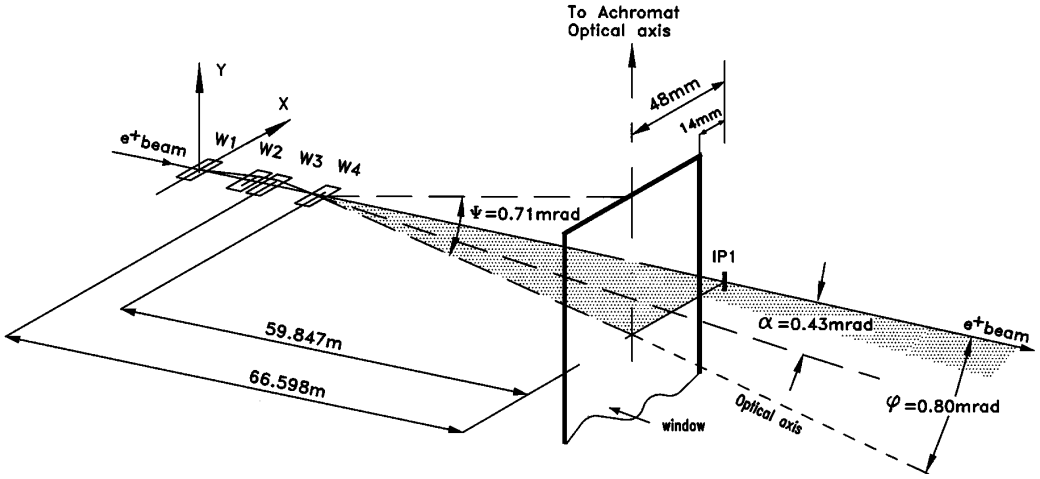

Figure 6: Main characteristics of the imaging optics set up. The window at 60 m from W4 symbolizes the extraction mirror. The optical axis from W4 to the streak camera makes an angle φ= 0.8 mrad with the LEP beam axis.

2.3 Numerical simulation of residual interference effects

A major goal when decreasing the destructive interferences between W3 and W4 by pulling them apart (see Ref. [4] and Appendix 2) from 0.76 m (center to center; Fig. 1) up to 6.75 m (Fig. 4), is to produce a SR beam significantly more intense than the parasitic light from other sources.

Numerical simulations of the residual interference phenomena have been performed using the ray-tracing code ZGOUBI [6] of which a typical input data file is given in Appendix 3. A typical result is given in Fig. 7 which shows the E_σ and E_π components of the double electric field impulse radiated by a single electron travelling in W3 and W4 as observed at a very large distance along the imaging optics axis. Figure 8 shows the corresponding frequency spectra $dP_\sigma/d\nu d\Omega$ and $dP_\pi/d\nu d\Omega$, as a function of the photon energy $\omega = h\nu$ where ν is the radiation frequency, Ω the observed solid angle.

The spectral range relevant to the use of the streak camera is in the very low-frequency domain $\omega \approx$ 1.55–3.1 eV. In this frequency interval $dP/d\nu\Omega$ is rapidly oscillating, with frequency [4] $\omega \simeq 2c/d/[(\varphi+\alpha)^2+\alpha^2/8] \simeq 0.28$ eV, hence the streak camera averages the power, which result in an overall $\sim$ 2 residual loss factor w.r.t. the single dipole case, over the mirror acceptance.

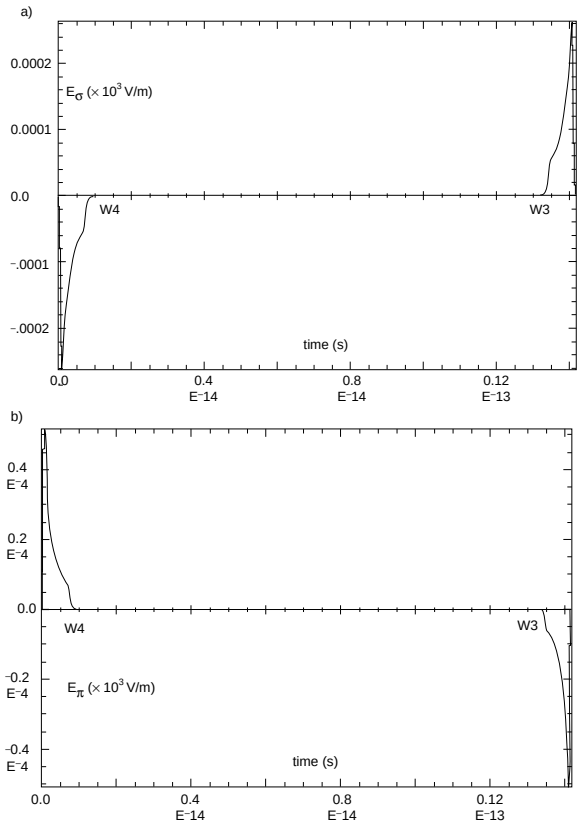

Figure 7: Numerical simulation of the double electric field impulse radiated by a single electron on a LEP bunch-train mode closed-orbit bump in W3 and W4 as observed at large distance in the direction of the imaging optics (assumed to be at $\varphi = 0.67$ mrad):
a) E_σ component (parallel to the LEP orbit plane),
b) E_π component (orthogonal).
The time interval between the two impulses is $T \simeq \frac{d}{2c}[(\varphi+\alpha)^2 + \frac{\alpha}{8}^2] \simeq 1.42 \times 10^{-14}$ s with $d = 6.75$ m, $\alpha = 0.43$ mrad, $\varphi = 0.67$ mrad, $c =$ speed of light.

3 Experimental results

3.1 General results

The first comparative measurements between the original mini-wiggler set-up (Fig. 1) and a configuration where the SR emission from a single dipole could be observed were performed in 1993. In the former case the light intensity was comparable to that from the parasitic sources (e.g. QL4) while in the latter case a grey filtering attenuation of more than 2 orders of magnitude was needed to reproduce the former intensity level. This result suggested that the interference effects could be cured on the basis of the theoretical investigations [4].

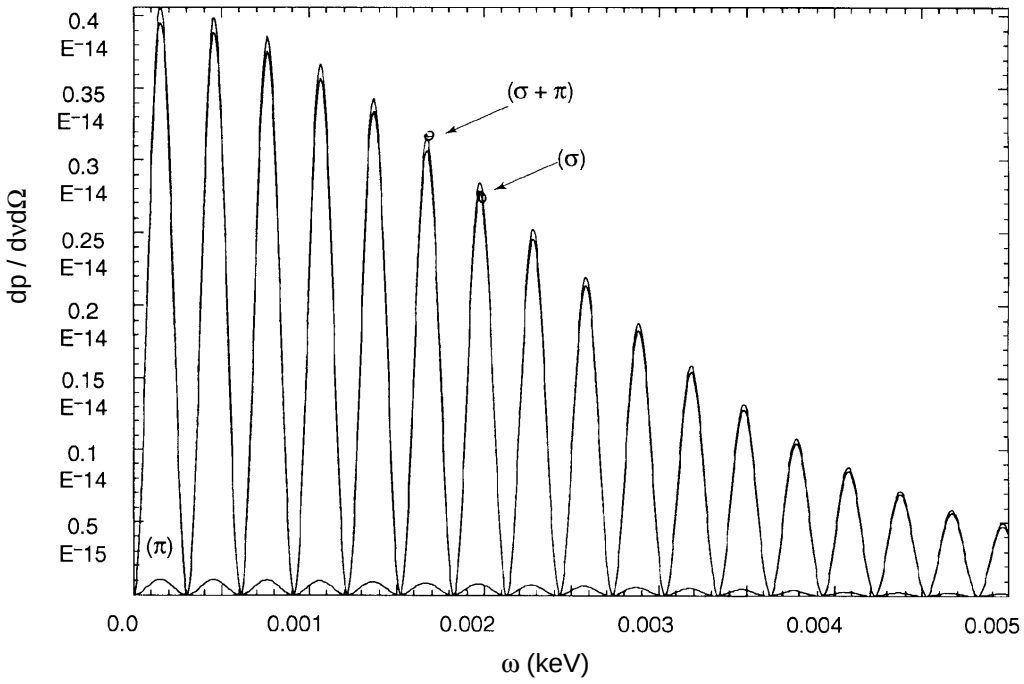

Figure 8: Spectral angular brightness $dP_\sigma/d\nu d\Omega$, $dP_\pi/d\nu d\Omega$ and their sum (ν = frequency, Ω = solid angle) plotted against the photon energy $\omega = h\nu$ (keV), radiated by a single electron on a LEP bunch-train mode closed-orbit bump in W3 and W4, as detected at large distance in the direction of the imaging optics. The range of interest for the streak camera is in the lower part of the spectrum from about 1.55 to 3.1 eV (400–800 nm), large enough w.r.t. the rapidly oscillating interference, therefore resulting in an averaging which reduces the interference loss to a residual factor ~ 2 w.r.t. the single dipole case, over the mirror acceptance. The amplitudes are normalized to 1 mA circulating e-beam current neglecting effects from finite emittance.

Several experiments have been performed in 1995 using this new configuration (Figs. 4, 5) and the results can be summarised as follows.

A preliminary result was that the SR intensity from the W3–W4 pair compared fairly with the single dipole case with a remaining factor of ~ 2 in the interference intensity loss as predicted from the numerical simulations for the case of a pair of dipoles 6 m apart (Appendix 2). It is worth to mention that following the improvements in the production of visible light a series of accelerator physics experiments requiring the use of the streak camera could be successfully performed with a very low (4 μA) single bunch current.

In the next step a good alignment of the imaging optics was realized. This, in particular, allowed to adjust the focusing by moving the achromat lenses over the whole available range of ~ 0.75 m while keeping the images aligned along the optical axis. Preliminary tests showed that the image from W3 was well focused at the nominal position on the optics bench. The image from W4 could then be focused by adjusting the achromat lens to its extreme position.

Intensity measurements as a function of the deflection α were performed making use of polarising filters to separate the σ- and the π-components of the radiation. As a consequence of the small e-beam emittance the usual two lobes of the π-component [9] were clearly observed on a screen positioned slightly out of focus. This method was adopted to precisely determine the longitudinal position of the image plane defined by the superposition of these two π-lobes.

The images from W3 and W4 were successfully separated by increasing the bump amplitude up to $\sim$ 9.3 mm at 20 GeV ($\alpha \sim 1.38$ mrad, $I = 40$ A, see Table 1). Moreover the images of the two other sources W1, W2 could also be observed by tuning the mini-wiggler to $\alpha = -1.4$ mrad at 20 GeV (opposite sign bump).

The results, described in the next section, were found in good agreement with the expected behaviour of the set-up geometry.

3.2 Intensity measurements

A machine development session was devoted to the acquisition of images from W4 with a CCD camera. The images, digitised and saved on files for further analysis, are collected in Fig. 9.

The acquisition system software includes automatic contrast (gain) and brightness (offset) control, which has been taken into account in order to obtain the integrated intensities. Details of the numerical treatment of the images can be found in [8] . The results are summarised in Table 2 which gives the integrated intensity of the σ and π polarisation components of the visible synchrotron radiation at the camera in arbitrary units, for three different excitation currents.

Table 2: Integrated intensities of the light spots of Fig. 9. In the case of the images corresponding to 40 A excitation it was possible to measure the W4 and W3 light spots separately (Figs. 9.1 and 9.2). The integrals obtained for the other images correspond to a combination of the light from the 2 sources. Beam energy $E = 20$ GeV.

Source	I (A)	α (mrad)	σ-component	π-component	$\sigma + \pi$	σ/π
W3	40	1.40	0.80	0.13	0.93	6.2
W4	40	1.40	0.86	0.20	1.06	4.3
W3+W4	25	0.88	2.39	1.71	4.10	1.4
W3+W4	12	0.42	1.53	0.85	2.38	1.8

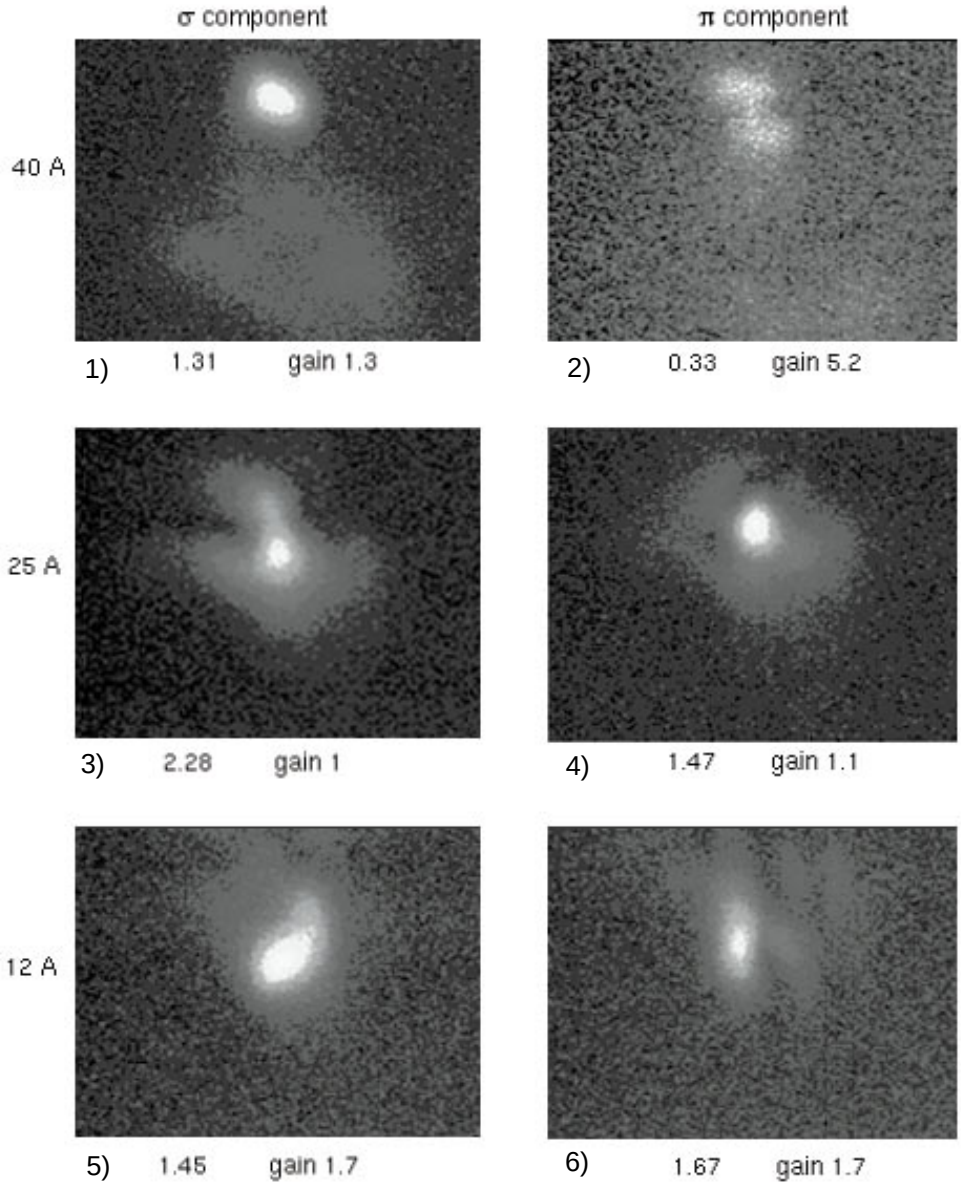

Figure 9: A series of photographs illustrating the experimental results obtained in 1995. Note that the horizontal axis in the photographs is the vertical axis in LEP. Each of the 3 rows corresponds to a given current in the mini-wiggler dipoles W3 and W4 (I = 12, 25 and 40 A). The left-hand column shows the light spots for the σ-component and the right hand column the ones for the π-component. The value under each image gives the integrated light intensity obtained in arbitrary units. These values are compared with the theoretical calculations on Fig. 10. At 12 and 25 A the light spots due to W3 and W4 overlap, while at 40 A they are well separated. As expected, at 40 A the light spot of W3 is out of focus with a maximum intensity of about 10% that of W4 (see Appendix 1).

These values are compared with the theoretical predictions on Fig. 10. At 12 A and 25 A (Figs. 9.3–9.6) the light spots due to W3 and W4 overlap, while at 40 A (Figs. 9.1 and 9.2) they are well separated and can be measured directly.

As expected the light spot of W3 is out of focus with a maximum density of about 10% that of W4 (Appendix 1).

The double spot along the horizontal direction (φ-angle of Fig. 11) in the π image on Fig. 9.2 is attributed to the edge effect [4, 10], each spot being due to respectively the entrance and exit edge radiation in W4 (Fig. 11), while the contribution of the magnet body is negligible (left column of Fig. 12); no such double spot is observable in the σ-component, seemingly in contradiction with the σ edge-peaks seen in Figs. 11 and 12: these are in fact simply not perceptible due to the weakness of the contrast (a factor of ~ 2) between the edge and body radiated intensities.

Note that the integrated intensity of the image of W3 is about $0.93/1.06 \simeq 88\%$ that of that of W4. One would expect this value to be in the ratio of the squares of the distances of the sources to the achromats, namely $(81.3/88.1)^2 \sim 85\%$ (Table 1), which is in good agreement.

3.3 Numerical simulations

Figure 10 presents a comparison between these results and the theoretical predictions given in Figs. 11 and 12 which display the shape of the σ- and π-components of the visible SR at the surface of the extraction mirrors at IP1.

A major feature of the simulations is that they involve the single SR source W4, thus neglecting any residual interference effects due to W3. Such interferences would result in a distortion of the SR spectrum by a partial sine-modulation (Appendix 2) which in turn would translate into non-linear effects in Fig. 10, where the light power as a function of the dipole excitation is implicitely correlated to the overlapping of the two sources W3 and W4 (Fig. 9).

The intensity measurements do not prove the existence of such residual interferences. Nevertheless the slight discrepancies between the measurements and the simulations might reveal it.

This point would deserve deeper experimental and theoretical investigations. It might for instance explain the fringes that appear in the π-spot of the W3–W4 image at 12A (Fig. 9.6).

As well, special properties as emphasised in the caption of Fig. 12 (such as $\int E_\sigma dt = 0$ at $\varphi = \alpha$) need finer experimental insight. Investigations relevant with this issue have been performed recently at ESRF [13].

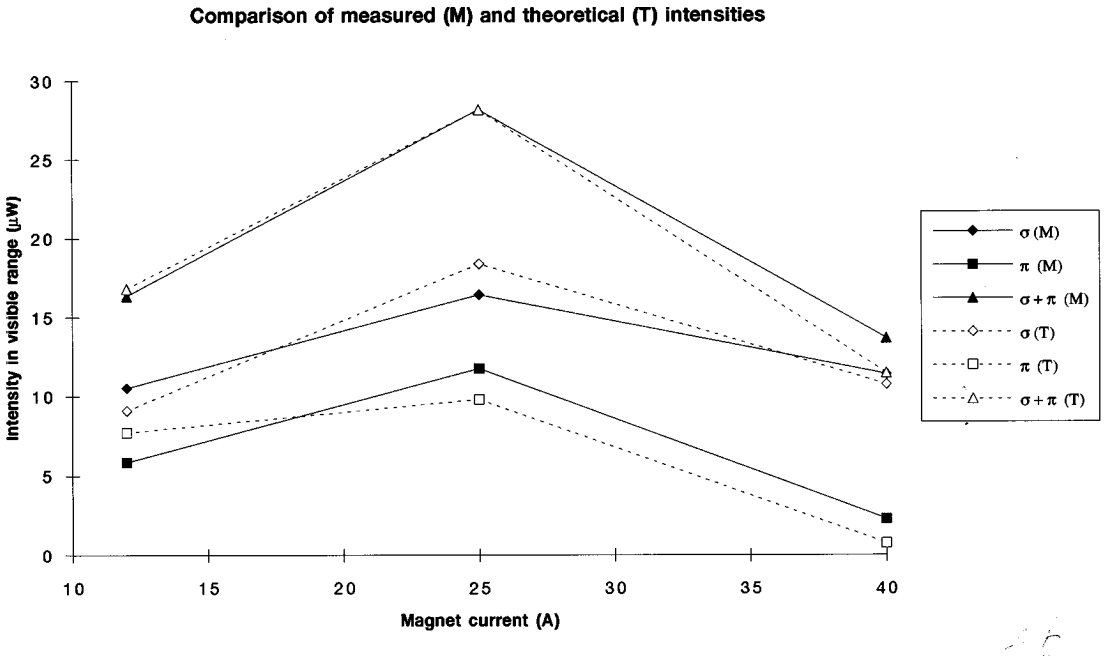

Figure 10: Comparison between the measured intensities detailed in Figure 9 and the values obtained from the numerical simulations for a 1 mA, 20 GeV electron beam, in the 400–800 nm spectral range. The measured data have been normalised to the values calculated for the total $\sigma + \pi$ intensity at 25 A.

4 Conclusions

A new configuration of the dedicated SR source (mini-wiggler) compatible with the LEP2 energies and the bunch train scheme is now in operation. Pulling the last two dipoles 6.75 m apart considerably reduces the destructive interference of the two sources and improves the light intensity by a factor of about 30 compared to the previous configuration.

These experimental results confirm the predictions from theoretical investigations and provide a deeper insight into the problem of interference phenomena in connection with the emission of synchrotron radiation from small dipoles. This might be of particular importance for the optimisation of LHC beam diagnostics [14] where the same codes will be used to simulate the brightness of a short dipole in the spectral range beyond the critical energy.

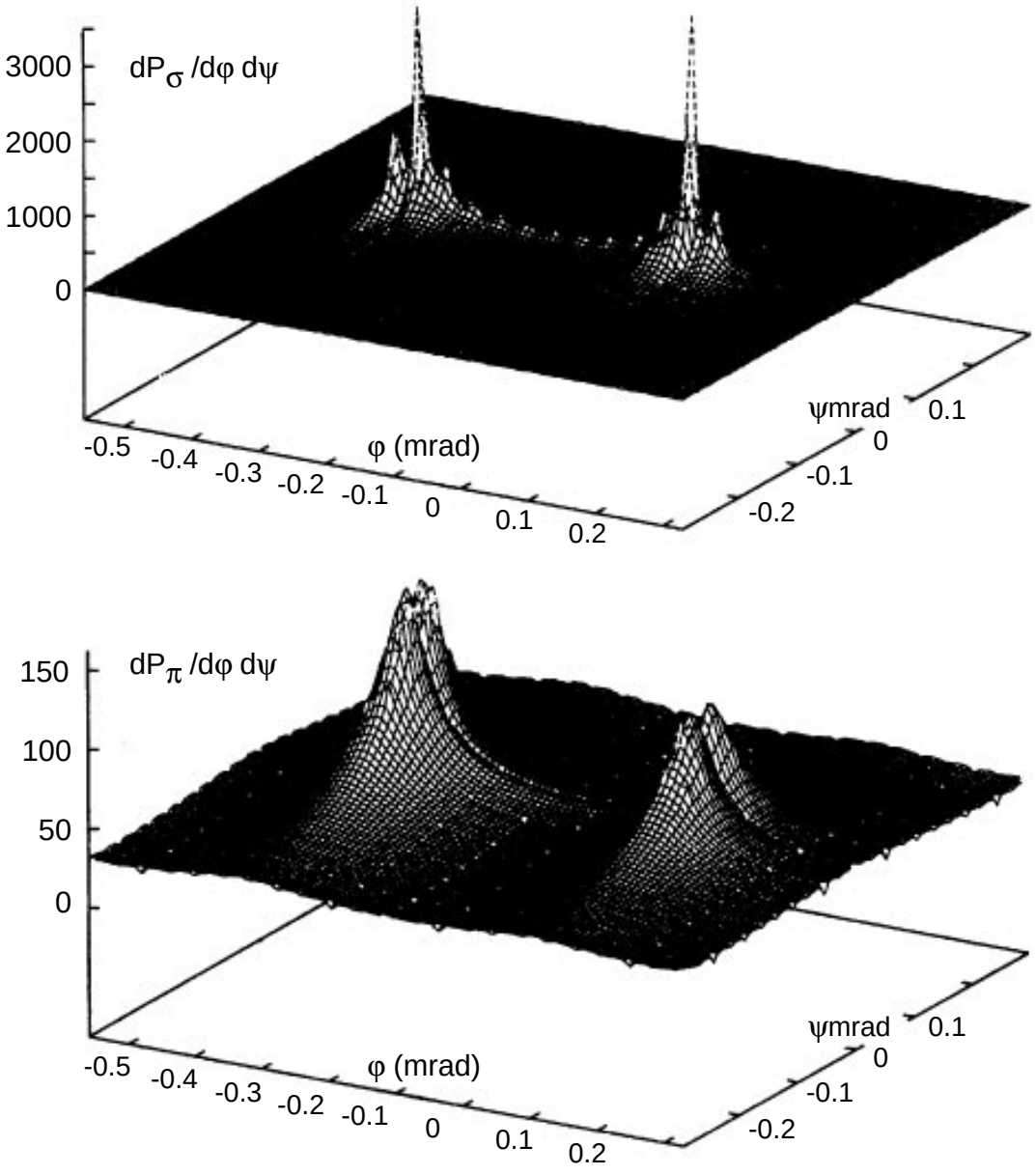

Figure 11: 3-D plot of the σ- and π-components of the visible light intensity (400–800 nm) from W4 at 20 GeV, α= 0.43 mrad, in the plane of the extraction mirrors (at IP1, Fig. 1). The transverse axes are the angles φ (horizontal) and ψ (vertical) defined in Fig. 6. The end intensity peaks are due to the edge radiation [4],[10] and can be interpreted in terms of the values of the time integrals $\int E_\sigma dt$ and $\int E_\pi dt$ (see Ref. [11] and Appendix 6 of ref. [4]).

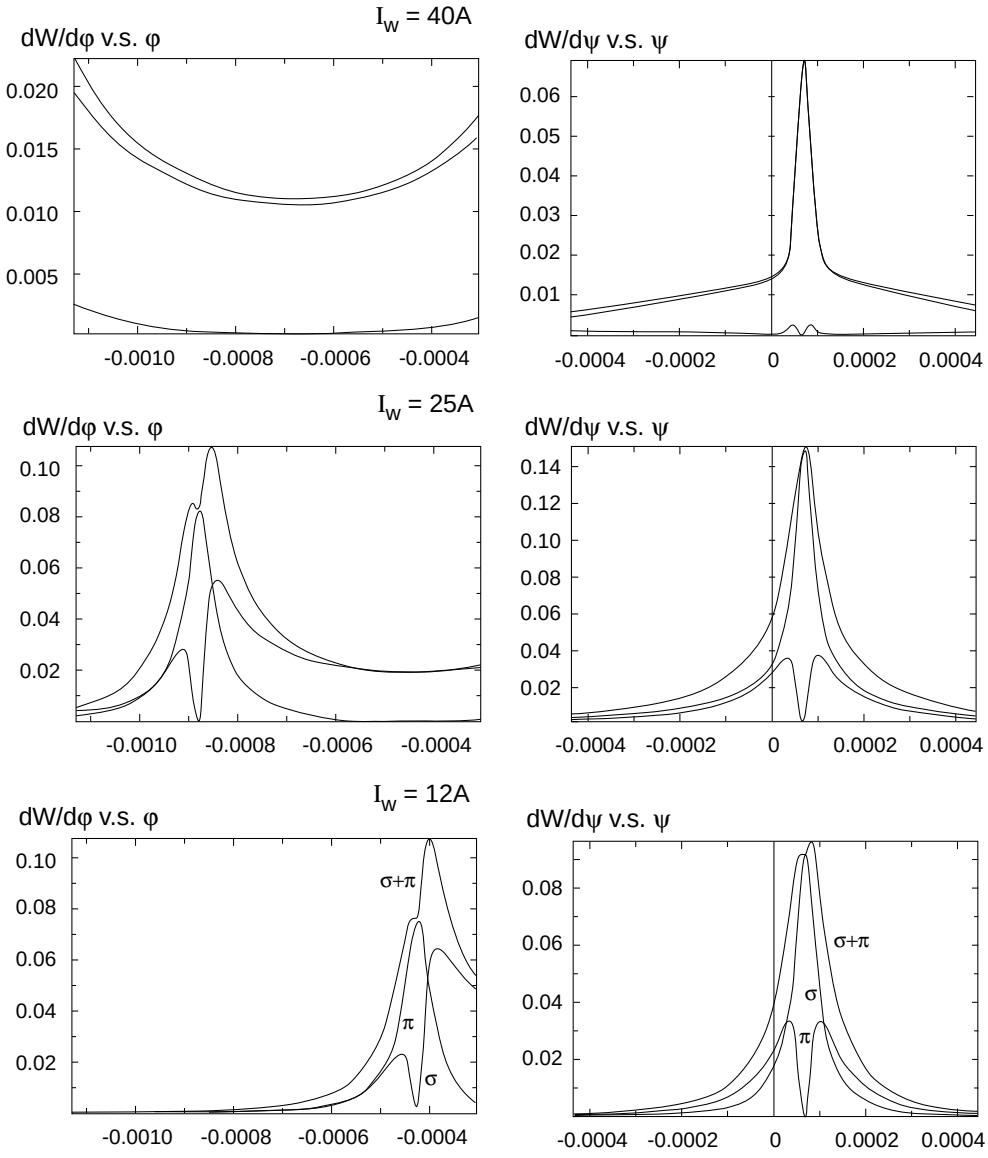

Figure 12: Projection of the σ- and π-components of the visible light distribution (of Fig. 11) onto a mirror surface limited to $-1.13 < \varphi < -0.5$ mrad and $-0.45 < \psi < .45$ mrad (as defined in Fig. 6) for the three different dipole exitations 12 A, 25 A and 40 A, as due to a 20 GeV electron, nomalized to 1 mA beam current. These plots can be directly compared to those of Fig. 9 It can be observed that the vertical projections (right-hand column) are off-centered at $\psi \sim 0.07$ mrad : this is due to the non-zero vertical closed orbit in the bunch-train mode [5]. It can also be observed that the P_σ/P_π ratio varies strongly from one dipole excitation to the other, and is however very different from the usually admitted (2/3)/(1/3) ratio of the low frequency classical SR approximation [9]. Finally, it can be verified that the density $dP_\sigma/d\varphi$, and hence $\int E_\sigma dt$, is zero for $\varphi = \alpha$ (namely, $\varphi = \alpha = 0.43$ mrad at 12 A, and $\varphi = \alpha = 0.88$ mrad at 25 A).

References

[1] C. Bovet, M. Placidi, A dedicated synchrotron radiation source for LEP beam diagnostics,
LEP Note 532, CERN, 11/4/85.

[2] E. Rossa, F. Tecker, J.C. Mathae, Performance limits of a streak camera in real time three-dimensional measurement of bunch oscillation in LEP,
Preprint of 1993 PAC, May 17–20, Washington, D.C.

[3] K. Hanke, Measurements of the bunch length of LEP with a streak camera and comparison with results from LEP experiments,
CERN SL/Note 95–65 (BI), CERN, 13/06/95.

[4] F. Méot, Synchrotron radiation interferences at the LEP mini-wiggler,
CERN SL/94–22 (AP), CERN, 28/06/94.

[5] C.Bovet *et al.,* Final Report of the 1994 Bunch Train Study Group,
CERN SL/94–95 (AP), CERN, 21/12/94.

[6] F. Méot and S. Valéro, ZGOUBI users' guide,
Report LNS/GT/93–12, CEA, Saclay, 1993.

[7] Closed orbit scheme due to A. Verdier, CERN/SL/AP 1993.

[8] A.J. Burns, Measurement of intensity of synchrotron light spots for different mini-wiggler currents,
CERN SL/Note 97–38 (BI), CERN, 29/04/97.

[9] A. Hofmann, Theory of synchrotron radiation,
SLAC report, SSRL-ACD Note 38, Sept. 1986, p. 32.

[10] O. Chubar, and N.V. Smoliakov, Kurtchatov Institute, preprint AE–5596/14 (1992).

[11] E.G. Bessonov, On a class of electromagnetic waves, Zh. Eksp. Teor. Fiz. 80, 852–858 (March 1981).

[12] J. Bosser et al., Characteristics of the radiation emitted by pand $\bar{p}$ in an undulator, J. Phys. Lett. 45 (1984) L–343–351.

[13] C. Denise, Etude de la lumière synchrotron èmise par des quadrupôles et des champs de fuite de dipôles. Intérêt pour le diagnostic machine, Rapport de Thèse, Université Paris XI et ESRF, 11 Septembre 1996.

[14] J. Bosser, C. Bovet, R. Jung, Preliminary studies on aprofile monitor for the LHC using SR, LHC/Note 192, 17 June 1992.

Appendix 1 – Optical field depth in the new configuration

The imaging optics intercepts the SR from W3 and W4 and focuses it onto the image plane related to W4, creating a blurred image of W3 which produces a quasi-constant 10% background. This can be understood and quantified as follows. We consider two point sources situated at W3 and W4 and calculate the size of the extended image of W3 onto the image plane of W4 due to the effect of the field depth neglecting all geometrical and chromatic aberration.

Off-focus imaging

We refer to Fig. 13. The imaging optics consist of a single achromat doublet [1] symbolised by a converging thin lens of focal length f. Let p_4 (p'_4) the distance from W4 (its image $W4'$) to the achromat lens, and p_3 (p'_3) be the distance from the latter to W3 (its image $W3'$). We can write

$$p'_{\mathrm{i}} = \frac{p_{\mathrm{i}}\ f}{p_{\mathrm{i}} - f} \quad , \quad (\mathrm{i} = 3{,}4) \ . \tag{2}$$

Let θ'_3 be the refracted angle from W3. The blurring of the image of W3 at the plane of $W4'$ is then

$$\Delta W3' = 2\ \theta'_3 (p'_4 - p'_3) = 2\ \theta'_3\ \Big(\frac{p_4\ f}{p_4 - f} - \frac{p_3\ f}{p_3 - f}\Big) \tag{3}$$

With the new set-up values (Table 2) $p_3 = 68$ m , $p_4 = 61$ m , $f = 15.7$ m

$$\Delta W3' \approx 1.5\ \theta'_3 \sim 1.5\ \theta_3\ \Big(\frac{p_3}{p'_3}\Big) \sim 1.5\ \theta_3\ \Big(\frac{p_3 - f}{f}\Big) \ . \tag{4}$$

It is also possible to write the blurring $\Delta W3'$ as a function of the dipole current I as well as of the deflection angle α as follows.

SR opening angle

The non-bend plane of the SR source practically coincides with the vertical plane of LEP, since the vertical closed-orbit angle is very small in the bunch-train mode (Appendix 3 and Ref. [5]). Neglecting this effect we can write the vertical r.m.s opening angle of the SR cone, energy independent in the low-frequency approximation, for the contribution of both SR polarisation components as [9]:

$$\sigma_{\theta_3} = 0.83\ \Big(\frac{\lambda}{2\pi\rho}\Big)^{1/3} = 0.83\ \Big(\frac{\alpha\lambda}{2\pi L}\Big)^{1/3} \ , \tag{5}$$

where λ is the observed wavelength and L the dipole magnetic length.

With the numerical values from Table 2 we get for the vertical r.m.s opening angle of the SR cone at $\lambda = 600$ nm

$$\sigma_{\theta_3} = 0.35 \text{ mrad} \ .$$

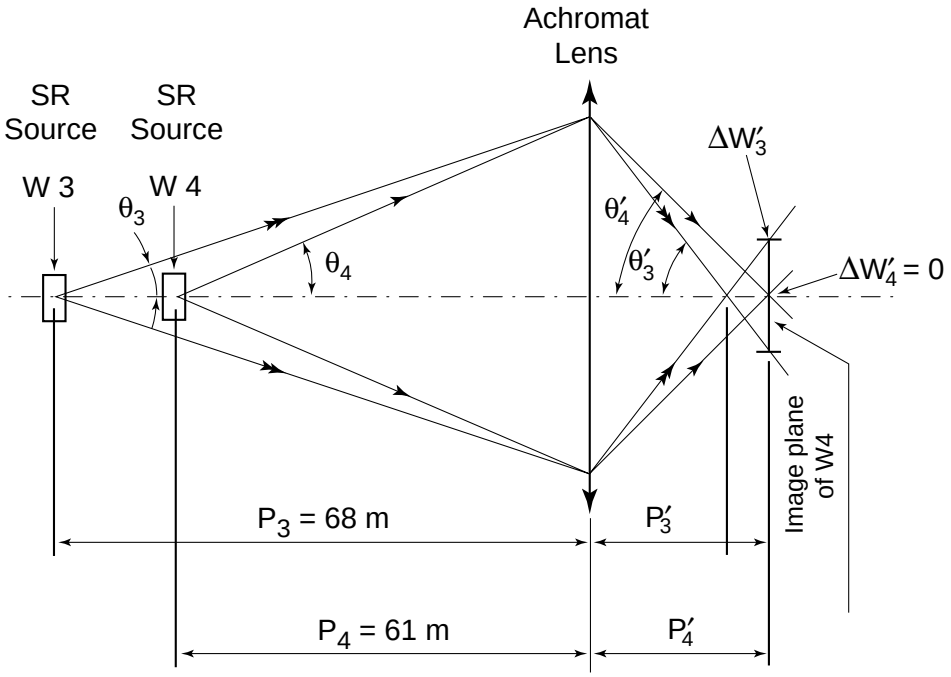

Figure 13: A scheme of the imaging of W3 onto the image plane of W4s howing the effect of the field depth.

These considerations concern the depth of field effects for the vertical component of the SR angular brightness. The horizontal r.m.s opening angle is enhanced by the effect of the horizontal sweep of the beam, which tends to reduce the field depth. We can thus restrict the study to the effect of the vertical opening as quantified above, which gives a lower limit for the expected blurring of the parasitic source W3.

Off-focus image of W3

We now consider that the light from W3 has a bell-shaped, quasi-Gaussian angular distribution with an r.m.s opening σ_{θ_3}. Since the transverse position $W3'$ of a ray at the image plane is proportional to its initial angle θ'_3 both have the same probability density function with the unique difference of a scaling factor i.e. $W3'$ is Gaussian with an r.m.s width

$$\sigma_{W3'} = 1.5\ \sigma_{\theta_3}\ \left(\frac{p_3 - f}{f}\right)\ .$$

Taking $p_3 = 68$ m, $f = 15.7$ m and $\sigma_{\theta_3} = 0.35$ mrad we have for the r.m.s size of the extended image of W3 on top of the point-like image of W4:

$$\sigma_{W3'} \sim 1.7 \text{ mm}\ .$$

Effect of the field depth on the image size

The effect on the relative change of the image size can be quantified by taking into account the object size (namely the finite transverse cross section $\sigma_{x,y}$ of the circulating electron beam) and the diffraction effects [1]:

$$\sigma_{\mathrm{x,y}} = 0.5 \text{ mm} \ , \ \sigma_{\mathrm{diffr}} = 0.24 \text{ mm} \ .$$

We then get for the r.m.s. size of the image of W4 at ~ 20 m from the achromat:

$$\sigma_4 = \frac{20}{61} \ \sqrt{\left(\sigma^2_{\mathrm{x,y}} + \sigma^2_{\mathrm{diffr}}\right)} = 0.18 \text{ mm}$$

and for the image of W3:

$$\sigma_3 = \sqrt{\left(\frac{20}{68}\right)^2 \ \left(\sigma^2_{\mathrm{x,y}} + \sigma^2_{\mathrm{diffr}}\right) + \sigma^2_{W3'}} = 1.7 \text{ mm} \ .$$

Both sources W3 and W4 emit the same amount of power, but W3 is attenuated with respect to W4 by a factor

$$r = \left(\frac{p_4 + p'_4}{p_3 + p'_4}\right)^2 \sim \left(\frac{81}{88}\right)^2 \sim 0.85$$

and we have, considering the peak intensities I_3 and I_4 at the image plane,

$$I_3 \ \sigma_3 \approx r \ I_4 \ \sigma_4$$

and hence

$$\frac{I_3}{I_4} \approx r \ \frac{\sigma_4}{\sigma_3} = 0.85 \times \frac{0.18}{1.7} \approx 10\% \ .$$

Appendix 2 – The SR interferences in the mini-wiggler set-up

Figure 14 shows [4] the double electric field impulse emitted by a 45 GeV electron undergoing a deflection $\alpha = \pm 0.43$ mrad in W3 and W4 (left column) and the corresponding brightness $dP_\sigma/d\nu d\Omega$ (normalised to a 1mA circulating beam current) in the direction $\varphi = \alpha/2$ (right column), for two different values of the distance W3 to W4 (for more results see Appendixes 2–5 of Ref. [4]).

Similar interference phenomena, with edge radiation have been investigated in detail at the CERN/Sp$\bar{p}$S [12].

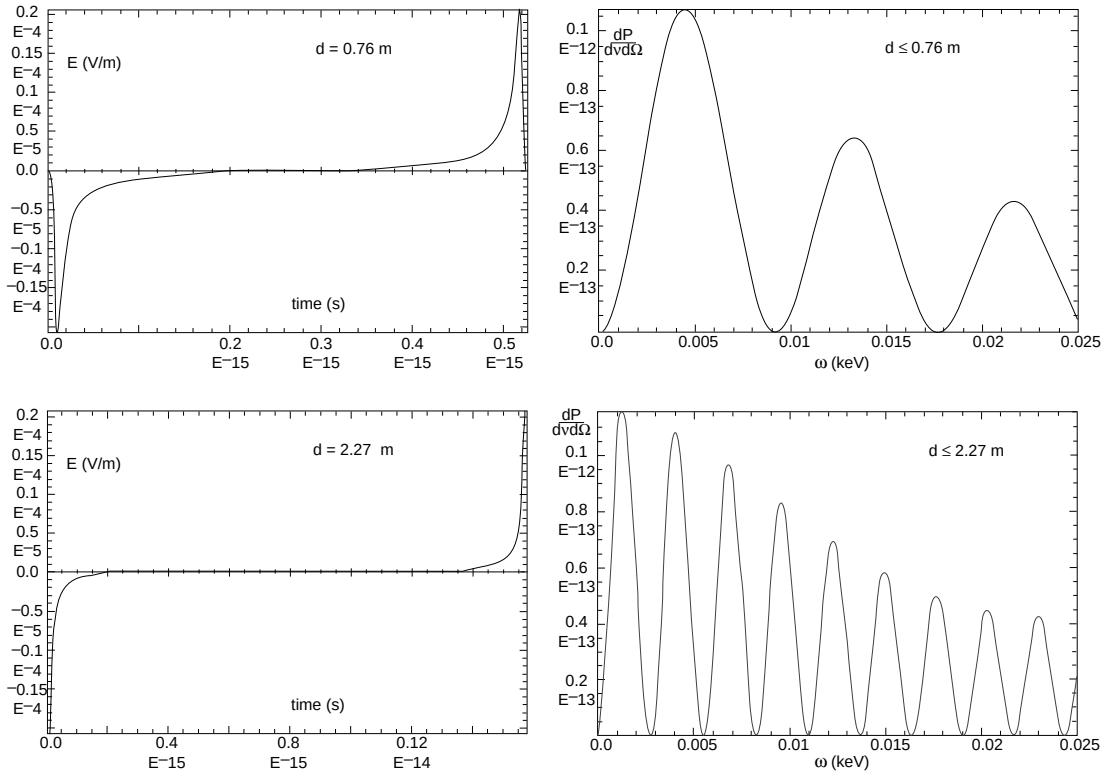

Figure 14: Double electric field impulse emitted by a 45 GeV electron undergoing a α= 0.43 mrad deflection in W3 and W4 (left column) and the corresponding brightness $dP_\sigma/d\nu d\Omega$ (normalized to 1 mA circulating beam current) in the direction $\varphi = \alpha/2$ (right column) for different values of the distance W3–W4.

Appendix 3 – A typical input data file for the code ZGOUBI

The initial coordinates of the particle launched into the mini-wiggler are that of the bunch-train closed orbit [5].

LEP MINI WIGGLER. Configuration 05/95; bunch train optics

```
'OBJET'
150103.8428                                  Rigidity (kG.cm) – 45 GeV electrons
2
1  1
0. 0. -.76453 .068273 0. 1. '0'             Incoming particle on closed orbit,
1                                            at WIG3M
'MULTIPOL'                                   WIG3M
2
52.602 10. 5.7071534 0. 0. 0. 0. 0.
10. 10.00 0. 0. 0. .0 .0
6 .1122 6.2671 -1.4982 3.5882 -2.1209 1.723
10. 10.00 0. 0. 0. 0. 0.
6 .1122 6.2671 -1.4982 3.5882 -2.1209 1.723
0. 0. 0. 0. 0. 0.
1000.200e10
1 0. 0. 0.
'FAISCEAU'
'ESL'
622.498
'MULTIPOL'                                   WIG4M
2
52.602 10. -5.7071534 0. 0. 0. 0. 0.
10. 10.00 0. 0. 0. 0. 0.
6 .1122 6.2671 -1.4982 3.5882 -2.1209 1.723
10. 10.00 0. 0. 0. 0. 0.
6 .1122 6.2671 -1.4982 3.5882 -2.1209 1.723
0. 0. 0. 0. 0. 0.
1 0. 0. 0.
'FAISCEAU'
```